Composite Structures 224 (2019) 111014

Contents lists available at ScienceDirect

Composite Structures

journal homepage: www.elsevier.com/locate/compstruct

Elastoplastic thermal buckling of functionally graded material beams

Jinghua Zhang*, Like Chen, Yali Lv

School of Science, Lanzhou University of Technology, Lanzhou, Gansu 730050, PR China

ARTICLE INFO

Keywords:
Functionally graded materials
Elastoplastic
Thermal buckling
Symplectic method

ABSTRACT

Elastoplastic thermal buckling characteristics of ceramic-metal functionally graded material (FGM) beams subjected to transversely non-uniform temperature rise are investigated by symplectic method in Hamiltonian system. Based on TTO model, the linear hybrid hardening elastoplastic model is used to simulate the elastoplastic material properties and establish thermal elastoplastic constitutive equations of FGM beams. Then, the canonical equations are established to transform critical loads and buckling modes into symplectic eigenvalues and eigensolutions in symplectic space. The main contributions of this study are that complete buckling mode space and critical thermal axial forces for elastoplastic thermal buckling of the FGM beams are obtained by analytical solutions; meanwhile, buckling temperatures and elastoplastic interfaces of the bucked FGM beams are obtained by inverse solutions. Numerical examples of buckling behaviors varying with thermal load, slenderness ratio and power law index are presented. The effects of elastoplastic material properties on critical temperatures and plastic zone are analyzed and discussed.

1. Introduction

Functionally graded materials (FGM) are advanced composite materials whose material properties vary smoothly and continuously in a certain direction and have been used in many engineering fields due to their excellent thermal resistance and crack resistance in extreme thermal environments [1,2]. When FGM structures are subjected to thermal loading, the variations of temperature result in thermal stresses even occurrence of instability.

Up to now, considerable research works on buckling and thermal buckling for FGM beams, plates and shells have been published, but most of them are only limited to elastic analyses. For example, buckling and post-buckling of FGM Timoshenko beams rested on two-parameter non-linear elastic foundation and under thermal loads were numerically investigated by Sun et al. [3]. Thermal buckling and post-buckling responses of FGM Timoshenko beams and imperfect plates under non-uniform heating were examined by Li et al. [4,5]. The results showed the behaviors of FGM beams and perfect plates with fixed boundaries are bifurcation buckling even if the non-uniform heating load is applied. However, the imperfect plates have no bifurcation buckling under any load. On the basis of isogeometric analysis and higher-order shear deformation theory, Tran et al. [6] examined the nonlinear thermomechanical stability of the FGM plate. Feldman and Aboudi [7] studied the bifurcation buckling of FGM rectangular plates subjected to in-plane loading. But the coupling between tension and bending of FGM plate was not considered, and also the condition of bifurcation buckling. Na and Kim [8], Liew et al. [9] studied the thermal buckling and thermal post-buckling of FGM rectangular plates. Ma and Wang [10] studied the post-buckling of FGM circular plates under mechanical and thermal loads on the basis of first-order and third-order plate theory. Studies had shown post-buckling equilibrium paths of FGM plates under static loading are stable. Najafizadeh and Eslami [11] studied the static thermoelastic stability of FGM circular plates on the basis of classical theory and Terriftz criterion. Sun et al. [12,13] studied the static thermal buckling of FGM cylindrical shells in symplectic space of Hamiltonian system, and the symplectic solution process were presented.

Engineering structures often suffer dynamic loads which lead to instability. Research on elastic dynamic stability of FGM structures, Ng et al. [14] discussed dynamic stability of FGM cylindrical shells subjected to harmonic axial loading. Sofiyev [15–17] solved the dynamic stability problem of FGM truncated conical shells under aperiodic impulsive loading and dynamic axial pressure, considering different initial conditions. These studies found the critical buckling loads can be effectively controlled by appropriately changing the volume fraction of FGM. Sohn and Kim [18] studied the static and dynamic stability of FGM panels under static thermal load and aerodynamic load, on the basis of first-order nonlinear plate theory. Prakash et al. [19] and Ganapathi [20] studied the dynamic stability of FGM shallow spherical shells under step load, and obtained the axisymmetric buckling critical loads via B-R criterion. Shariyat [21] analyzed the nonlinear dynamic

* Corresponding author at: Department of Engineering Mechanics, Lanzhou University of Technology, Lanzhou, Gansu 730050, PR China.
E-mail address: zjhhrb@163.com (J. Zhang).

https://doi.org/10.1016/j.compstruct.2019.111014
Received 15 February 2019; Received in revised form 27 April 2019; Accepted 20 May 2019
Available online 23 May 2019
0263-8223/

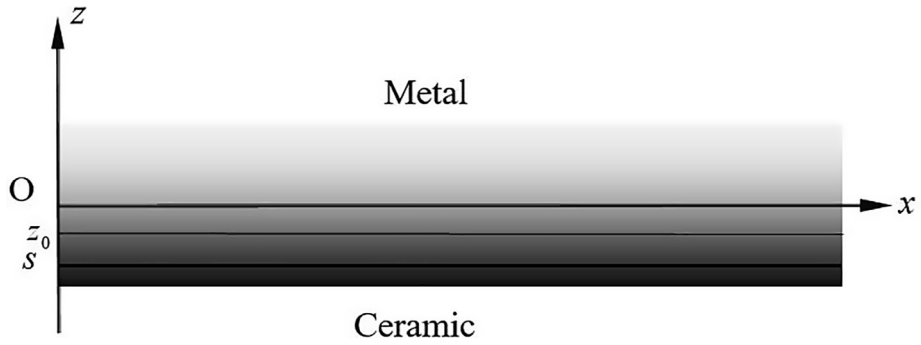

Fig. 1. Functionally graded material beam.

buckling characteristics of preloaded FGM cylindrical shells subjected to transient thermal. He also examined the dynamic buckling behaviors of FGM plates subjected to thermal, electric and mechanical loads [22]. Geometrical imperfections were considered in above two investigations. Ke and Wang [23] examined dynamic stability of FGM microbeams, considering size effect. Based on B-R buckling criterion, Huang and Han [24] researched the buckling of imperfect FGM cylindrical shells under axial compressed load on the basis of Donnell shell theory. Zhang and Li [25] studied nonlinear dynamic buckling of FGM conical shells under non-uniform normal mechanical impact loads, and the critical loads were obtained based on B-R buckling criterion. The static and dynamic buckling problems for imperfect FGM beams under uniform temperature rise load and compression were studied by Ghiasian et al. [26], considering temperature dependent and elastic foundation. Dynamic buckling load and post-buckling equilibrium path were presented.

If thicknesses of engineering structures are large, internal stresses are often large, even exceeding elastic limits. At the same time, since metals which are important constituents of FGM are plastic materials, they cause plastic deformation in regions with large stresses and elastoplastic buckling of FGM structures. With the increasingly wide utilization of FGM and higher safety requirements, it is necessary to examine elastoplastic buckling characteristics in order to more accurately predict the critical loads and improve permissible loads in elastic analysis, and also use plastic properties of materials fully. However, the research on elastoplastic buckling of FGM structures is much fewer compared to those on elastic buckling. Based on the Donnell shell theory and J_2 flow or deformation constitutive equations of FGM, the elastoplastic buckling of FGM cylindrical shells under axial compression, combined compression and pressure or torsional load were studied in Refs. [27–29], respectively. In which, Galerkin method was applied to solve the buckling equations, and solutions of critical load and regions of elastic, elastoplastic and plastic buckling were given. Using the same method, post-buckling of axial compressed elastoplastic FGM cylindrical shells were also examined by Xu et al. [30]. In addition, elastoplastic buckling and post-buckling of FGM plates under thermo-mechanical loads were studied by Sharma and Kumar [31,32], according to first-order shear and nonlinear plate theory. Elastoplastic post-buckling of FGM beams under mechanical load was studied by Trinh et al. [33], considering nonlinear elastic foundation. These studies show elastic post-buckling equilibrium paths of FGM plates and beams are stable, but those of elastoplastic post-buckling are unstable.

FGM beams are based on flexible design for their material properties. They achieve the expected functional requirements and satisfy the applications in various engineering field, such as aerospace, micromachines, nuclear power, information engineering and marine engineering etc. As far as the authors know, few research results have been reported on the elastoplastic thermal buckling of FGM structures. Therefore, this study examines the elastoplastic thermal buckling of ceramic-metal FGM beams by symplectic method in Hamiltonian system. The volume fractions of constituent materials are assumed to smoothly vary by power law function in the thickness direction and linear hybrid hardening elastoplastic model is used to simulate the elastoplastic material properties. The elastoplastic constitutive equations are established based on TTO model, in which ceramic is considered to be elastic and the metal is bilinear elastoplastic. And then canonical equations are established in Hamiltonian system and buckling mode equations and bifurcation conditions are solved by analytical methods; the buckling modes and buckling thermal loads are obtained accordingly. Finally, critical buckling temperatures and relevant elastoplastic interfaces are obtained via yield condition and inverse solutions of buckling thermal axial forces. Their influencing factors are also discussed in detail by parametric studies, this study provide a complete reference for the engineering design of FGM beams.

2. Problem formulations

Rectangular section FGM beams with length l, width b, height h and cross-sectional area $A = b \times h$ are considered, as schematically shown in Fig. 1. A coordinate system (x, y, z) is adopted where the x-axis is in axial direction, the y-axis in width direction and the z-axis in thickness direction. The xOy plane is placed on geometric midplane of the beams. The origin of coordinates is located at the centroid of left end. The FGM beams are subjected to transversely non-uniform temperature rise. The elastoplastic thermal buckling of FGM beams with fixed or pinned boundaries is considered.

2.1. Material properties of FGM

FGM are usually made of metal and ceramic. The effective material properties usually are predicted by micromechanical models such as the Mori-Tanaka estimates [34], the self-consistent, generalized self-consistent or differential schemes [35]. It should be mentioned the average field schemes are originally developed for statistically homogeneous aggregates on the basis of a representative volume element (RVE). However, there is no RVE to be defined in FGM, these average field estimates can only be applied with a reasonable degree of confidence. In addition, rule of mixtures [36] and the modified rule of mixtures have been developed to determine the effective properties of FGM. Although the rules of mixtures are simple and rough micromechanical models, they are widely used due to its simplicity and convenience. In this study, the linear rule of mixtures is also considered to describe variation of material properties, which beneficial to solve thermal conducted equations and obtain analytical solutions of stretching, bending-stretching coupling and bending stiffness coefficients. Based on the model, the material properties $P(z)$ of functionally graded materials (including mass density ρ, thermal expansion coefficient α, thermal capacity C and thermo-conductivity K) are expressed in compact form as [36]

$$P(z) = (P_c - P_m)V_c(z) + P_m \tag{1}$$

in which P_c and P_m indicate the material properties of ceramic and

metal, respectively. Volume fractions $V_c(z)$ and $V_m(z)$ are assumed to be power function of the thickness coordinate z [25], expressed as

$$V_c(z) = \left(\frac{h-2z}{2h}\right)^n, \quad V_m(z) = 1 - V_c(z) \tag{2}$$

in which power law index n is employed to control the distributions of constituents in FGM, and also measured the gradient characteristics of FGM.

For the elastoplastic material properties of ceramic-metal FGM (including elastic modulus E, yield limit σ_Y and tangent modulus H) are given based on the linear hardening elastoplastic model which is currently and widely accepted, named Tamura-Tomota-Ozawa (TTO) hybrid reinforcement model [30]. Generally, ceramics are brittle materials with higher elastic modulus and strength than those plastic materials. Therefore, we consider that the ceramics always maintain elastic deformations, and yield in FGM structures is mainly caused by the metals with bilinear elastoplastic when the equivalent stresses are greater than yield limit. Based on TTO model, elastic modulus, yield limit and tangent modulus of FGM can be given separately by the following expressions [30]

$$E = \left(\frac{q+E_c}{q+E_m}E_mV_m + E_cV_c\right)\Big/\left(\frac{q+E_c}{q+E_m}V_m + V_c\right) \tag{3}$$

$$\sigma_Y = \sigma_{Ym}\left(V_m + \frac{q+E_m}{q+E_c}\frac{E_c}{E_m}V_c\right) \tag{4}$$

$$H = \left(\frac{q+E_c}{q+H_m}H_mV_m + E_cV_c\right)\Big/\left(\frac{q+E_c}{q+H_m}V_m + V_c\right) \tag{5}$$

In the above formulas, E_m, H_m and σ_{Ym} represent elastic modulus, tangent modulus and yield limit of the metals, respectively. E_c represent elastic modulus of the ceramics. And $q = q'E_c$ is the ratio of stress to strain transfer, where q' is the stress transfer coefficient. $q' \to 0$ and $q' \to \infty$ correspond to the Reuss and the Voigt models, respectively. In this study, the Voigt model is used in numerical calculations, that is $q' \to \infty$.

2.2. Fundamental equations

For FGM beams under the transversely non-uniform temperature rise, their deflections at any point are denoted by w relevant to the z directions. According to the Euler–Bernoulli beam theory, normal strain ε_x is

$$\varepsilon_x = (z - z_0)\cdot\kappa \tag{6}$$

in which $\kappa = -\frac{\partial^2 w}{\partial x^2}$ indicates curvature at any point on the x axis. z_0 refers to the distance of physical neutral plane from geometric midplane of the beams shown in Fig. 1, and it is approximately calculated by

$$z_0 = \frac{\int_{-h/2}^{h/2} zE(z)\mathrm{d}z}{\int_{-h/2}^{h/2} E(z)\mathrm{d}z} \tag{7}$$

We consider that boundaries of FGM beams are fixed two ends (fixed-fixed, usually abbreviated to F-F) and fixed at one end and pinned at another end (fixed-pinned, abbreviated to F-P). For the F-F beams, when $x = 0$ and $x = l$, boundary conditions are

$$w|_{x=0,l} = 0, \quad \left.\frac{\mathrm{d}w}{\mathrm{d}x}\right|_{x=0,l} = 0 \tag{8}$$

For the F-P beams, when $x = 0$ and $x = l$, boundary conditions are

$$w|_{x=0,l} = 0, \quad \left.\frac{\mathrm{d}w}{\mathrm{d}x}\right|_{x=0} = 0, \quad \left.\frac{\mathrm{d}^2w}{\mathrm{d}x^2}\right|_{x=l} = 0 \tag{9}$$

For the elastoplastic FGM beams, there are the elastic deformation zone and the plastic deformation zone. The elastoplastic constitutive equations of the beams are described by TTO model combine with J_2 deformation theory. According to TTO model, relationships between axial normal stress σ_x and normal strain ε_x are [37]

$$\sigma_x = \begin{cases} E(z)[\varepsilon_x - \alpha(z)T(z)] & -0.5h \leqslant z < s \\ \sigma_Y(z) + H(z)\left[\varepsilon_x - \alpha(z)T(z) - \frac{\sigma_Y(z)}{E(z)}\right] & s \leqslant z \leqslant 0.5h \end{cases} \tag{10}$$

in which $T(z)$ is increment in temperature compared with ambient temperature T_0. s is the distance between elastoplastic interface and geometric midplane of FGM beams as shown in Fig. 1, its values are determined by external loads. When $s = 0.5h$, there is no plastic deformation inside FGM beams, therefore elastic buckling occurs. When $-0.5h < s < 0.5h$, elastoplastic buckling occurs. When $s = -0.5h$, can be seen plastic buckling occurs.

2.3. Canonical equation

In this study, Hamiltonian system and symplectic method are used in the elastoplastic buckling problem of the FGM beams subjected to transversely non-uniform temperature rise. The Lagrange function is

$$\overline{L} = E_k - \Pi = \frac{1}{2}I\left(\frac{\mathrm{d}w}{\mathrm{d}t}\right)^2 - \frac{1}{2}M_x\kappa - \frac{1}{2}N^T\left(\frac{\mathrm{d}w}{\mathrm{d}x}\right)^2 - \frac{1}{2}M^T\kappa \tag{11}$$

In the above formula, E_k and Π are kinetic energy and potential energy of FGM beams, respectively. $I = \int_A \rho(z)\mathrm{d}z$ is the mass per unit length. M_x, N^T and M^T separately are bending moment, thermal axial force and thermal bending moment, are defined as

$$M_x = \int_{A^e} E\varepsilon_x(z - z_0)\mathrm{d}A + \int_{A^p}\left[\sigma_Y + H\left(\varepsilon_x - \frac{\sigma_Y}{E}\right)\right](z - z_0)\mathrm{d}A$$

$$N^T = \int_{A^e} E\alpha T(z)\mathrm{d}A + \int_{A^p} H\alpha T(z)\mathrm{d}A \tag{12a}$$

$$M^T = \int_{A^e} E\alpha T(z)(z - z_0)\mathrm{d}A + \int_{A^p} H\alpha T(z)(z - z_0)\mathrm{d}A \tag{12b}$$

in which A^e is the cross-sectional area where elastic deformation occurs, A^p is the cross-sectional area where plastic flow occurs, and $A^e + A^p = A$. Introduce the problem into Hamiltonian system, define $w' = \frac{\partial w}{\partial x}$ and $\dot{w} = \frac{\partial w}{\partial t}$, then the Lagrange function can be expressed as

$$\overline{L} = \frac{1}{2}I\dot{w}^2 + \frac{1}{2}M_xw'' - \frac{1}{2}N^Tw'^2 + \frac{1}{2}M^Tw'' \tag{13}$$

Mark the original variable as $w = q$, and introduce dual variable

$$p = \frac{\delta\overline{L}}{\delta\dot{q}} = I\dot{q}$$

The Hamiltonian function can be expressed as

$$F = p\dot{q} - \overline{L} = \frac{p^2}{2I} - \frac{1}{2}M_xq'' + \frac{1}{2}N^Tq'^2 - \frac{1}{2}M^Tq'' \tag{14}$$

Introduce a state vector $\boldsymbol{\psi} = \{q, p\}^T$. Hamiltonian dual canonical equations can be derived by Legendre transformation and variational calculations as

$$\dot{\boldsymbol{\psi}} \equiv \begin{Bmatrix}\dot{q}\\ \dot{p}\end{Bmatrix} = \begin{Bmatrix}\frac{\delta F}{\delta p}\\ -\frac{\delta F}{\delta q}\end{Bmatrix} = \begin{Bmatrix}p/I\\ -D\frac{\mathrm{d}^4q}{\mathrm{d}x^4} - N^T\frac{\mathrm{d}^2q}{\mathrm{d}x^2}\end{Bmatrix} \tag{15}$$

In the above equation, D is bending stiffness of FGM beams, which is defined as

$$D = b\int_{-h/2}^{s} E(z - z_0)^2\mathrm{d}z + b\int_s^{h/2} H(z - z_0)^2\mathrm{d}z \tag{16}$$

The boundary conditions Eqs. (8) and (9) can also converted into Hamiltonian system. For the F-F FGM beams

$$q|_{x=0,l} = 0, \quad \left.\frac{\mathrm{d}q}{\mathrm{d}x}\right|_{x=0,l} = 0 \tag{17}$$

For the F-P FGM beams

$$q|_{x=0,l} = 0, \quad \left.\frac{\mathrm{d}q}{\mathrm{d}x}\right|_{x=0} = 0, \quad \left.\frac{\mathrm{d}^2q}{\mathrm{d}x^2}\right|_{x=l} = 0 \tag{18}$$

The Eqs. (15), (17), and (18) are the dual canonical equation and the boundary conditions for elastoplastic thermal buckling of FGM beams under non-uniform temperature in Hamiltonian system, which contain thermal axial forces that rely on the temperature fields. Therefore, solutions of the temperature fields have to be first acquired to solve the canonical equations.

3. Non-uniform temperature fields in FGM

The FGM beams are subjected to transversely non-uniform temperature rise, and the increments of temperature on upper surface and bottom surface are T_m and T_c, respectively. Four sides of the beam are adiabatic with environment. Due to the increments of transversely temperature inside FGM beams are assumed to be the function of thickness coordinate z, the increments $T = T(z)$ satisfy the following one-dimensional thermal conduction equation [4]

$$-\frac{\mathrm{d}}{\mathrm{d}z}\left[K(z)\frac{\mathrm{d}T(z)}{\mathrm{d}z}\right] = 0 \tag{19}$$

This model ignores the time of heat conduction, and the change of temperature due to work produced by the deformations is also neglected. However, the non-uniform temperature fields can be obtained easily by integrating Eq. (19) and using the boundary conditions $T(-h/2) = T_c$ and $T(h/2) = T_m$ as

$$T(z) = T_m\left[T_r + (1 - T_r)\int_{-h/2}^{z}\frac{1}{K(\eta)}\mathrm{d}\eta \Big/ \int_{-h/2}^{h/2}\frac{1}{K(z)}\mathrm{d}z\right] \tag{20}$$

in which $T_r = T_c/T_m$. Thermal axial force N^T with undetermined parameter T_c and T_m can be expressed by integrating Eq. (12a) in the thickness direction.

4. Analytical solutions of the equations

For the buckling problems of FGM beams in Hamiltonian system, zero eigenvalue and eigensolution satisfy the following equation

$$\dot{\boldsymbol{\psi}} = 0 \tag{21}$$

For easy solutions, dimensionless variables $X = x/l$, $L = l/h$, $W = w/l$, $Q = q/l$ and $\theta = \frac{N^T l^2}{D}$ are adopted. Then substituting them and Eq. (15) into Eq. (21), the dimensionless canonical equation can be written as

$$\frac{\mathrm{d}^4Q}{\mathrm{d}X^4} + \theta\frac{\mathrm{d}^2Q}{\mathrm{d}X^2} = 0 \tag{22}$$

The dimensionless boundary conditions also can be obtained as followings. For the F-F FGM beams

$$Q|_{X=0,1} = 0, \quad \left.\frac{\mathrm{d}Q}{\mathrm{d}X}\right|_{X=0,1} = 0 \tag{23a}$$

For the F-P FGM beams

$$Q|_{X=0,1} = 0, \quad \left.\frac{\mathrm{d}Q}{\mathrm{d}X}\right|_{X=0} = 0, \quad \left.\frac{\mathrm{d}^2Q}{\mathrm{d}X^2}\right|_{X=1} = 0 \tag{23b}$$

The Eq. (22) is a linear homogeneous equation whose general solution is

$$Q = C_1 + C_2X + C_3\cos(\sqrt{\theta}X) + C_4\sin(\sqrt{\theta}X) \tag{24}$$

where C_1, C_2, C_3 and C_4 are undetermined constants calculated via the boundary conditions. Substituting the boundary conditions Eq. (23a) of the F-F beams into Eq. (24) obtains

$$\begin{bmatrix} 1 & 0 & 1 & 0 \\ 0 & 1 & 0 & \sqrt{\theta} \\ 1 & 1 & \cos\sqrt{\theta} & \sin\sqrt{\theta} \\ 0 & 1 & -\sqrt{\theta}\sin\sqrt{\theta} & \sqrt{\theta}\cos\sqrt{\theta} \end{bmatrix}\begin{Bmatrix} C_1 \\ C_2 \\ C_3 \\ C_4 \end{Bmatrix} = 0 \tag{25}$$

For the boundary conditions Eq. (23b) of the F-P beams into Eq. (24) obtains

$$\begin{bmatrix} 1 & 0 & 1 & 0 \\ 0 & 1 & 0 & \sqrt{\theta} \\ 1 & 1 & \cos\sqrt{\theta} & \sin\sqrt{\theta} \\ 0 & 0 & -\theta\cos\sqrt{\theta} & -\theta\sin\sqrt{\theta} \end{bmatrix}\begin{Bmatrix} C_1 \\ C_2 \\ C_3 \\ C_4 \end{Bmatrix} = 0 \tag{26}$$

The solutions of Eqs. (25) and (26) should be non-zero while the elastoplastic buckling of FGM beams occurs, that is, determinants of coefficient matrices equal to zero. Expanding the determinants and simplifying equations to obtain the bifurcation conditions of elastoplastic thermal buckling. For the F-F FGM beams is

$$2 - 2\cos\sqrt{\theta} - \sqrt{\theta}\sin\sqrt{\theta} = 0 \tag{27}$$

For the F-P FGM beams is

$$\sin\sqrt{\theta} - \sqrt{\theta}\cos\sqrt{\theta} = 0 \tag{28}$$

The dimensionless buckling eigenvalues θ_i for the two kinds of boundary conditions can be calculated by solving Eqs. (27) and (28) using Newton-Raphson method, respectively. Based on the expressions $\theta = \frac{N^T l^2}{D}$, $N^T = \int_{A^e} E\alpha T(z)\mathrm{d}A + \int_{A^p} H\alpha T(z)\mathrm{d}A$ and $D = b\int_{-h/2}^{s} E(z - z_0)^2\mathrm{d}z + b\int_{s}^{h/2} H(z - z_0)^2\mathrm{d}z$, the relevant buckling temperature increments T_m^{cr} will be obtained.

In order to calculate the distances s between elastoplastic interface and geometric midplane, assume the strain at any point on cross-section is the same when FGM beams are in critical states of buckling, and equal to the strain at the yield point $\varepsilon_x = \sigma_Y(s)/E(s)$. The axis force N in cross-section of FGM beams is

$$\begin{aligned} N &= \int_{A^e}\sigma^e\mathrm{d}A + \int_{A^p}\sigma^p\mathrm{d}A \\ &= \int_{A^e}E(z)\varepsilon_x\mathrm{d}A + \int_{A^p}\left[\sigma_Y(z) + H(z)\left(\varepsilon_x - \frac{\sigma_Y(z)}{E(z)}\right)\right]\mathrm{d}A \end{aligned} \tag{29}$$

Considering the strain, Eq. (29) can be written as

$$N = \int_{A^e}E(z)\frac{\sigma_Y(s)}{E(s)}\mathrm{d}A + \int_{A^p}\left[\sigma_Y(z) + H(z)\left(\frac{\sigma_Y(s)}{E(s)} - \frac{\sigma_Y(z)}{E(z)}\right)\right]\mathrm{d}A \tag{30}$$

For the FGM beams that are only subjected to thermal loads, thermal axial forces equal to axial forces in the cross-sections. Substituting the obtained eigenvalues θ_i into $\theta = \frac{N^T l^2}{D}$ in combination with Eq. (30), the ith-order buckling thermal axial force and the relevant distance s can be obtained by numerically solving nonlinear algebraic equations. Furthermore, the ith-order buckling temperature increment can be obtained by inverse solving the equation $N^T = \int_{-h/2}^{s} E\alpha T(z)\mathrm{d}A + \int_{s}^{h/2} H\alpha T(z)\mathrm{d}A$.

The buckling modes can be obtained by the normalization method. Let $C_4 = 1$, and the other coefficients of buckling modes for the two kinds of boundary conditions are solved via Eqs. (25) and (26). For the F-F FGM beams obtain

$$C_1 = \frac{\sqrt{\theta_i} - \sin\sqrt{\theta_i}}{1 - \cos\sqrt{\theta_i}}, \quad C_2 = -\sqrt{\theta_i}, \quad C_3 = \frac{\sin\sqrt{\theta_i} - \sqrt{\theta_i}}{1 - \cos\sqrt{\theta_i}} \tag{31}$$

For the F-P FGM beams obtain

$$C_1 = tan\sqrt{\theta}, \quad C_2 = -\sqrt{\theta}, \quad C_3 = -tan\sqrt{\theta} \tag{32}$$

Then substituting the two sets of coefficients C_1, C_2, C_3 and C_4 into Eq. (24), the ith order buckling modes of FGM beams with two kinds of boundary conditions can be obtained. For the F-F FGM beams, are expressed as

$$Q_i = \frac{\sqrt{\theta_i} - sin\sqrt{\theta_i}}{1 - cos\sqrt{\theta_i}}[1 - cos(\sqrt{\theta_i}X)] + [sin(\sqrt{\theta_i}X) - \sqrt{\theta_i}X] \tag{33}$$

For the F-P FGM beams are

$$Q_i = \tan\sqrt{\theta_i}[1 - \cos(\sqrt{\theta_i}X)] + [\sin(\sqrt{\theta_i}X) - \sqrt{\theta_i}X] \tag{34}$$

5. Numerical results and discussions

5.1. Buckling modes of the FGM beams

The dimensionless eigenvalues for elastoplastic thermal buckling of FGM beams with two kinds of boundary conditions are obtained by bifurcation conditions Eqs. (27) and (28) using Newton-Raphson method. For the F-F beams, they are

$\theta_1 = 39.47$, $\theta_2 = 80.76$, $\theta_3 = 157.91$, $\theta_4 = 238.72$, $\theta_5 = 355.31$, … ;

For the F-P beams, they are

$\theta_1 = 20.19$, $\theta_2 = 59.67$, $\theta_3 = 118.90$, $\theta_4 = 197.85$, $\theta_5 = 296.55$, … .

Substituting the above eigenvalues into Eqs. (33) and (34) separately, the ith-order buckling modes of F-F and F-P FGM beams can be obtained. First- to fourth-order buckling modes of F-F and F-P FGM beams are plotted in Fig. 2a and b, respectively. As shown in the two figures, the different eigenvalues are corresponding to different buckling modes. The orders and wave numbers of buckling modes are increased with dimensionless characteristic values increasing. At the same time, it is found that the shapes of buckling modes are independent of the material properties by comparing with the results in Ref. [38].

5.2. Elastoplastic buckling thermal loads and yield interfaces

In this section, elastoplastic critical thermal axial forces and elastoplastic interfaces of the bucked FGM beams are calculated and discussed. Firstly, the accuracies of theoretical derivations and numerical calculations in this study are illustrated, and also the effectiveness of symplectic method to study elastoplastic thermal buckling of FGM beams. Let $s = h/2$, the elastoplastic FGM beams degenerate into fully elastic beams. At the same time, bending stiffness and thermal axial force become $D = b\int_{-h/2}^{h/2} E(z - z_0)^2 dz$ and $N^T = b\int_{-h/2}^{h/2} E\alpha T(z) dz$, respectively. When the power law index $n = 0$, the FGM beams are reduced into homogeneous beams. In this way, the critical buckling temperatures (i.e. the minimum buckling temperatures which corresponding to the first-order buckling mode $i = 1$) for homogeneous elastic beams can be obtained by symplectic method, in which the material properties are selected the same as in Refs. [4,39]. Comparisons between the present results and the corresponding results of Refs. [4,39,40] are separately listed in Table 1. In Ref. [4], the dimensionless thermal load parameter is $\lambda = L^2\alpha_m T_m$, the critical buckling temperature for F-F beam $\lambda_{cr} = 3.29$ can be obtained. In Ref. [40], the dimensionless thermal load parameter is $\tau = 12L^2\alpha T$, the dimensionless critical temperature for F-P beam $\tau_{cr} = 20.1907$ can be obtained. Converting these results above into dimensional critical temperatures, and then listing them and the results of Ref. [39] in Table 1. As shown in the table, the results obtained by symplectic method are very close to the results in Refs. [4,39,40] obtained by traditional method of elastic mechanics, it proves that the correctness and reliability of calculation by the symplectic method.

In the following numerical calculations, the length of FGM beam is specified as $l = 500$ mm. The constituent materials are considered as ceramic Zirconia and metal Ti-6Al-4V, material properties of them are listed in Table 2.

Fig. 3(a–c) demonstrate the variations of critical thermal axial forces for the F-F FGM beams with the power law index n, given different valuers of slenderness ratios $L = 5$, 10 and 15. As shown in the three figures, the critical thermal axial forces decrease when the power law index n increases. It means that the abilities of FGM beams to withstand axial forces decrease with the increase of n. This is because the FGM beams reduce to homogeneous ceramic ones when $n = 0$; And reduce to metal beams when $n \to \infty$. The constituents of the ceramics drop when n increases, so the Young's modulus, tangent modulus and bending stiffness of FGM beams decrease. At the same time, the critical thermal axial forces decrease obviously with the increase of smaller n; But for bigger n, the variations gradually decrease. In addition, we can found that when $n < 63$, $n < 6$ and $n < 1$ separately corresponding to the F-F FGM beams with slenderness ratio $L = 5$, $L = 10$ and $L = 15$, the failure forms are strength failure, and no buckling occurs. For $n \geqslant 63$, $n \geqslant 6$ and $n \geqslant 1$, the elastoplastic buckling of FGM beams with $L = 5$, $L = 10$ and $L = 15$ begins to occur. This is because that when n is small, the ceramic is the main constituent material of FGM, the elastic modulus of the beams is large, and the structures does not suffer from buckling failure. As n increases, the volume fraction of metal increases, and the bending stiffness decreases, so it results in the occurrence of

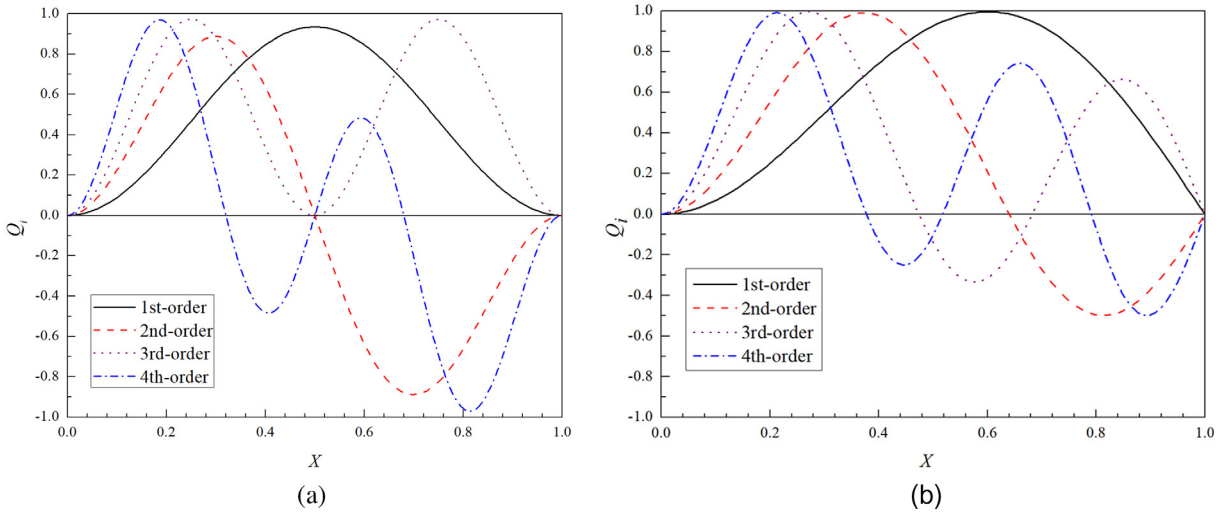

Fig. 2. 1st- to 4th-order buckling modes of the FGM beams. (a) F-F ends, (b) F-P ends.

Table 1
Critical temperatures of the homogeneous beam with F-F and F-P boundaries.

B.C.	L	10	15	20	25	30	40	50	60
F-F	Ref. [4]	1430.43	635.75	357.61	228.87	158.94	89.40	57.22	39.73
	Ref. [39]	1426.79	634.87	353.13	226.47	158.61	87.13	56.48	39.47
	Present	1430.07	635.59	357.52	228.81	158.90	89.38	57.20	39.72
F-P	Ref. [39]	728.15	328.18	182.27	121.02	81.84	47.48	31.61	19.91
	Ref. [40]	731.55	325.13	182.89	117.05	81.28	45.72	29.26	20.32
	Present	731.52	325.12	182.88	117.04	81.28	45.72	29.26	20.32

Table 2
Material properties of Zirconia and Ti-6Al-4V [41,42].

Material	K [W/(m·K)]	E (GPa)	α (1/K)	σ_Y (MPa)	H (MPa)
Zirconia	1.7	244.26596	12.7657×10^{-6}	–	–
Ti-6Al-4V	1.20947	122.55676	7.57876×10^{-6}	1540.93	2306.15

elastoplastic thermal buckling. In addition, since the bending stiffness of FGM beams decrease as the slenderness radio increases, the amount of critical buckling thermal axial forces drop significantly as the slenderness ratio increases which could be found by comparing the three figures.

Fig. 4(a, b) plot the variations of critical thermal axial forces N_{cr}^{T} for the F-P FGM beams with the power law index n, given slenderness ratios $L = 5$ and 10. As shown in these figures, the critical buckling thermal axial forces decrease when the power law index n increases. In addition, we can found that when $n < 23$ and $n < 2$ corresponding to the F-P FGM beams with slenderness ratio $L = 5$ and $L = 10$, the failure forms are strength failure, and no buckling occurs. For the F-P FGM beams with $L = 5$, the elastoplastic buckling begins to occur when $n \geqslant 23$. For $L = 10$, the elastoplastic buckling begins to occur when $n \geqslant 2$. Comparing with the Fig. 3(a–c), it can be found that the buckling critical forces of the F-F beams are larger than those F-P beams, when the same parameters n and L are given.

Characteristic curves of the distance s between elastoplastic interface and geometric midplane versus the power law index n are plotted in Fig. 5(a–c). When elastoplastic buckling of the F-F beams occurs, representing some specified values $L = 5$, 10 and 15. It can be found from the Fig. 5(a) that the distances s increase with increasing n, and it change slightly only between -50 and -47.5 for the F-F FGM beams with the slenderness ratio $L = 5$ when buckling occurs. It means that the elastoplastic interface is very close to the ceramic side, and slightly offset to the metal side with increasing n or the decrease of critical

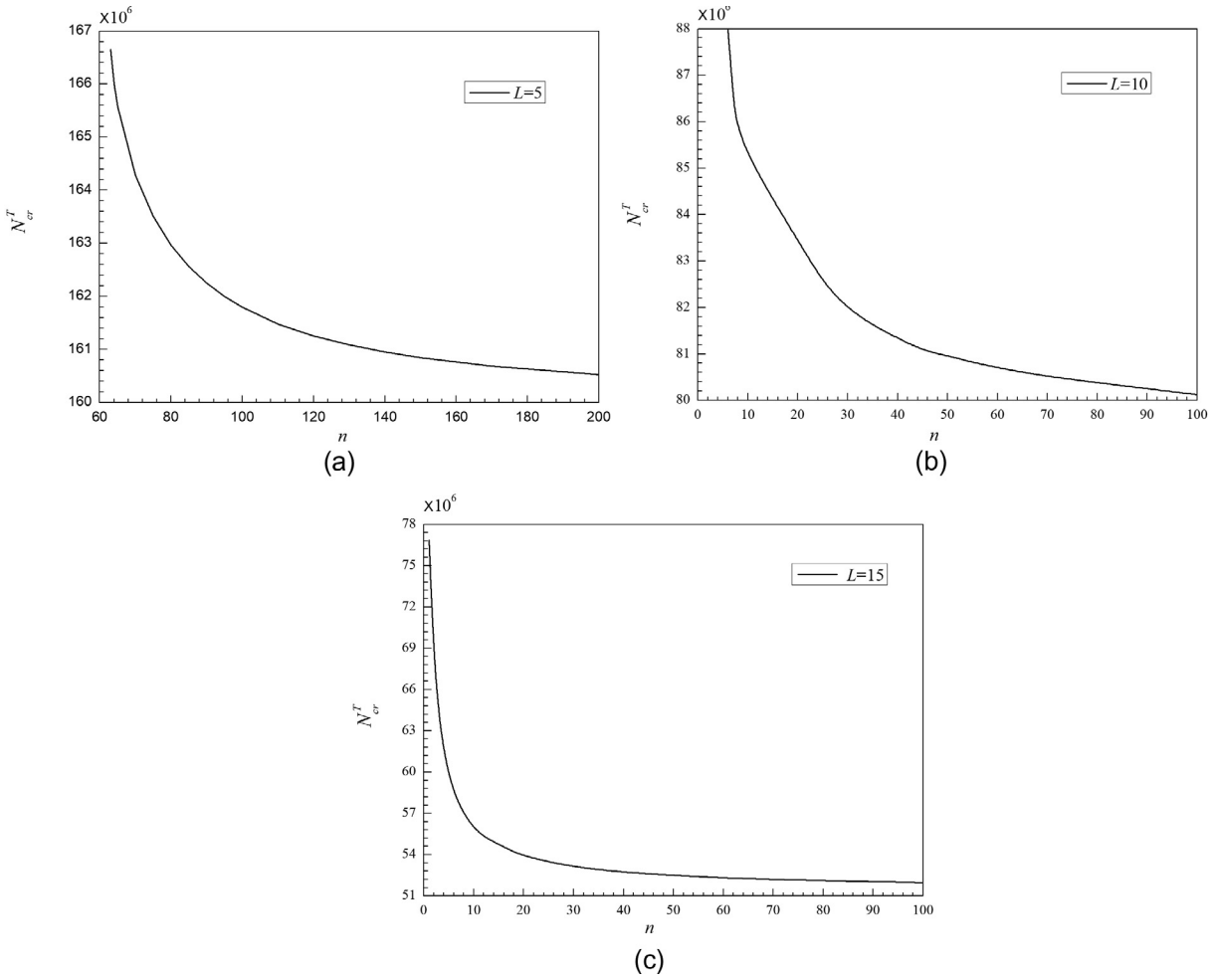

Fig. 3. The critical thermal axial forces N_{cr}^{T} of the F-F FGM beams versus power law index n. (a) $L = 5$, (b) $L = 10$, (c) $L = 15$.

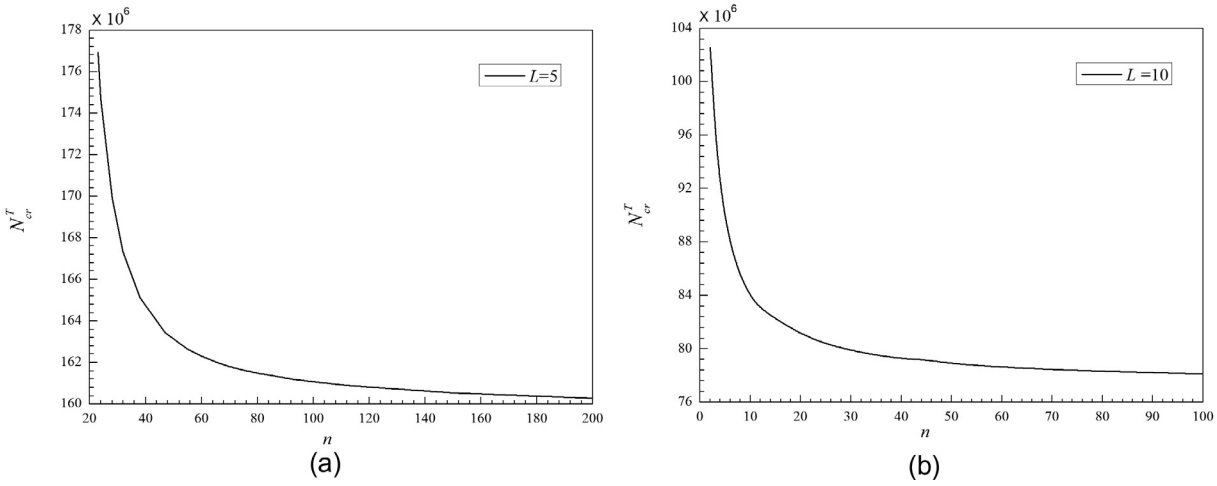

Fig. 4. The critical thermal axial forces N_{cr}^{T} of the F-P FGM beams versus power law index n. (a) $L = 5$, (b) $L = 10$.

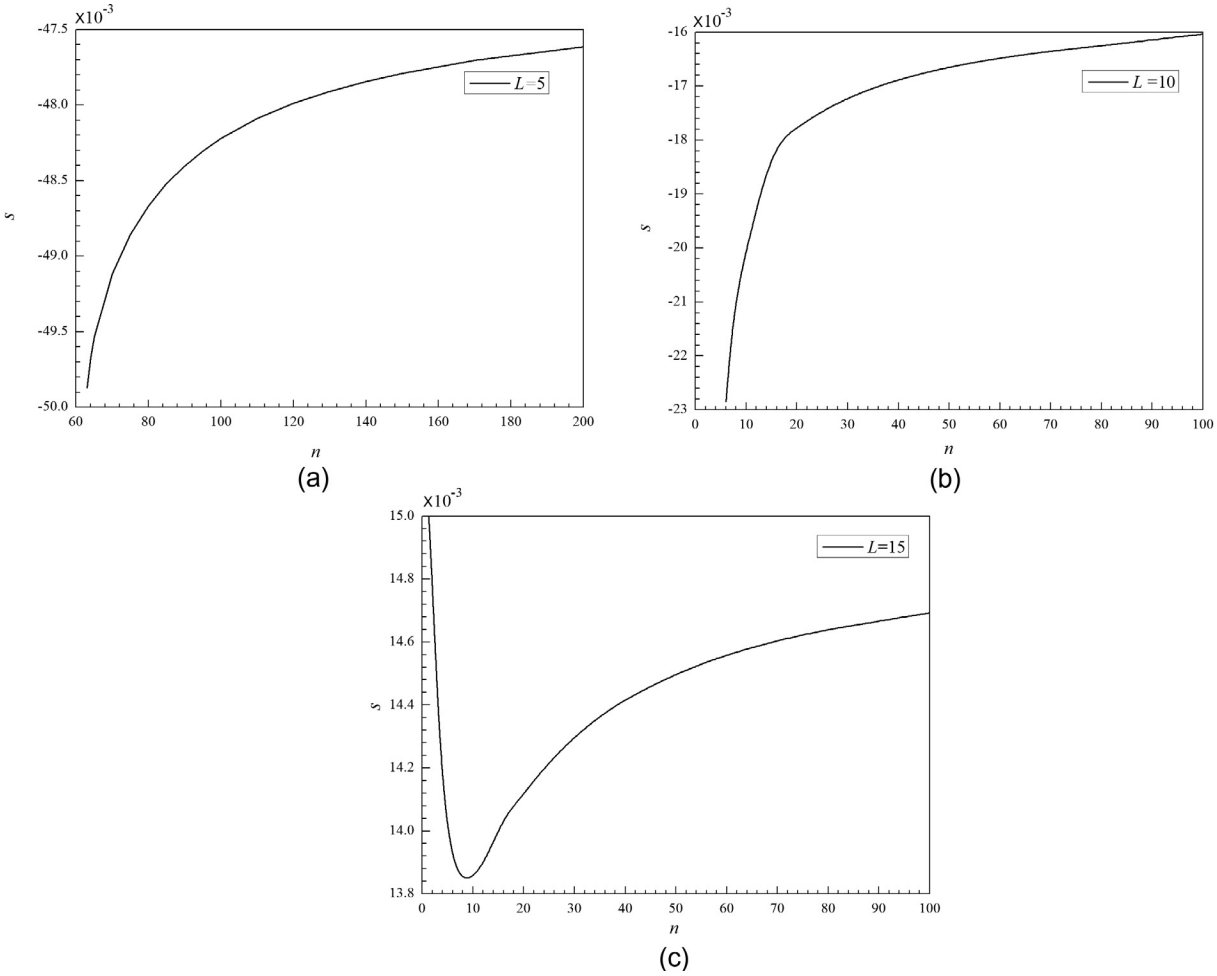

Fig. 5. The distances s of the elastoplastic interfaces for the bucked F-F FGM beams versus n. (a) $L = 5$, (b) $L = 10$, (c) $L = 15$.

thermal axial forces. Especially for bigger n, the positions of interface are almost motionless with the increase of n. It is indicated that for smaller slenderness beams, most of the stresses inside FGM beams exceeds yield limit when elastoplastic thermal buckling occurs. For the F-F FGM beams with $L = 10$, as shown in Fig. 5(b), the distance s increases with increasing n, i.e., the elastoplastic interface move from the ceramic side toward the metal side with increasing n. When n is large, the distances s increase very slowly, and eventually tend to be constant with the increase of n. It means that the plastic deformation zone is small when n is small or the volume fraction of the ceramic is large. As n increases or the volume fractions of the metal increase gradually, the plastic deformation zone also widen. The non-monotonic variations of s are because the metal in FGM beams increases and the critical thermal axial forces also decrease as n increases. For the beams with $L = 15$, the distance s varies only between 13.8 and 15. The elastoplastic interface is close to the metal side and moves in a small range with the increase of

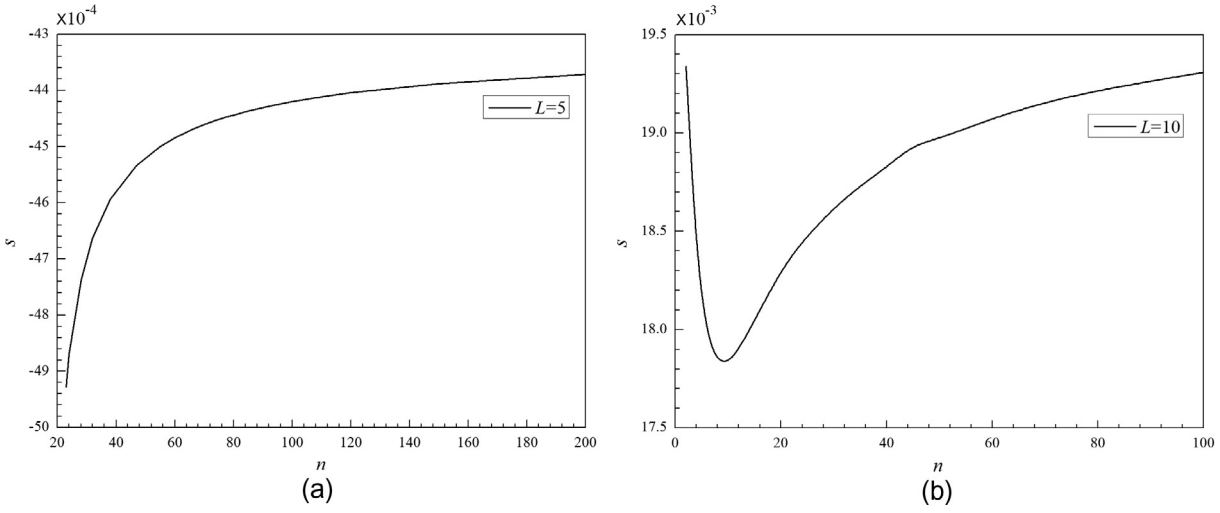

Fig. 6. The distances s of the elastoplastic interfaces for the bucked F-P FGM beams versus n. (a) $L = 5$, (b) $L = 10$.

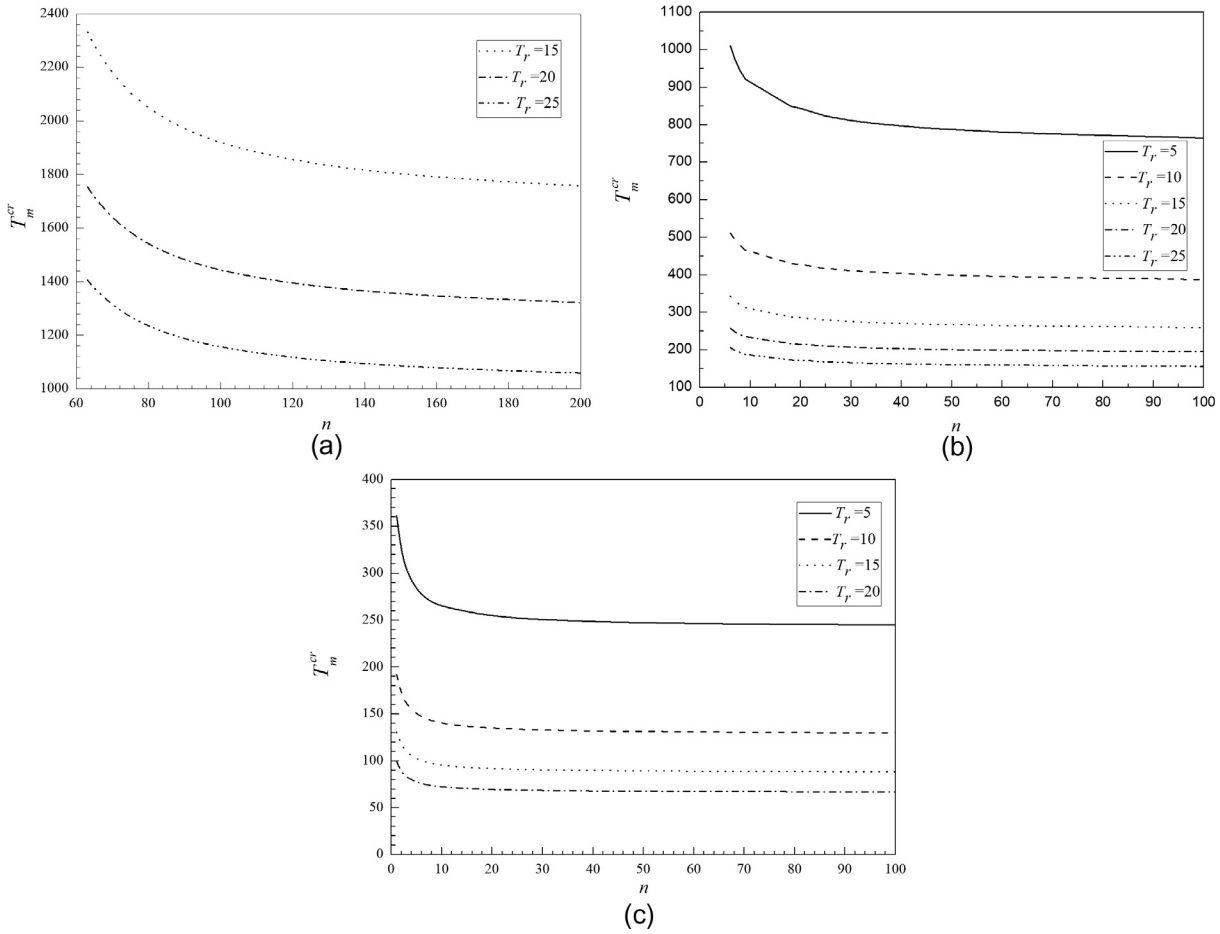

Fig. 7. The critical temperature T_m^{cr} of the F-F FGM beams versus power law index n. (a) $L = 5$, (b) $L = 10$, (c)$L = 15$.

n, it means that the plastic deformation zone is smaller.

Fig. 6(a, b) plot the variations of the distances s with n for the bucked F-P FGM beams. As shown in Fig. 6(a), law of the variations for the F-P FGM beams with $L = 5$ is similar to the F-F beams. The elastoplastic interface is close to the ceramic side and slightly offset to the metal side with increasing n or the decrease of critical thermal axial forces. Most of stresses inside the smaller slenderness FGM beams exceed yield limit when elastoplastic thermal buckling occurs. For the F-P FGM beams with $L = 10$, it can be found from Fig. 6(b) that the distance s varies only between 17.8 and 19.4. And the elastoplastic interface is close to the metal and varies in a small range with the increase of n, so the plastic deformation zone is smaller. Comparing with Fig. 5(a–c), we can found that the elastoplastic zones of the bucked F-P beams are smaller than the F-F beams, when the same parameters L and n are given.

Table 3
N_{cr}^{T} and T_m^{cr} of the F-F FGM beam with $L = 10$.

n		6	8	20	35	50	60	80	100
$N_{cr}^{T}(\times 10^6$ N)		87.98	85.55	83.46	81.62	80.96	80.71	80.38	80.12
T_m^{cr} (K)	$T_r = 5$	1010.95	943.67	843.33	803.32	787.52	780.95	772.34	764.55
	$T_r = 10$	512.29	478.12	427.42	407.25	399.28	395.97	391.62	387.69
	$T_r = 15$	343.07	320.17	286.25	272.76	267.44	265.22	262.32	259.69
	$T_r = 20$	257.88	240.67	215.18	205.05	201.05	199.39	197.20	195.23

Table 4
N_{cr}^{T} and T_m^{cr} of the F-F FGM beam with $L = 15$.

n		5	7	12	30	40	50	80	100
$N_{cr}^{T}(\times 10^6$N)		59.87	57.74	55.29	53.14	52.74	52.49	52.11	51.98
T_m^{cr} (K)	$T_r = 5$	282.56	272.65	262.48	250.63	248.62	247.39	245.51	244.88
	$T_r = 10$	149.76	144.46	138.32	132.92	131.89	131.26	130.30	129.98
	$T_r = 15$	101.87	98.26	94.09	90.44	89.75	89.33	88.69	88.47
	$T_r = 20$	77.19	74.45	71.29	68.54	68.01	67.70	67.21	67.06

5.3. Critical buckling temperatures

In this section, the critical buckling temperatures are calculated and discussed. And the influences of material gradient, parameters of structural geometry and thermal loadings on critical buckling temperatures are also studied. Fig. 7(a–c) show the variations of elastoplastic critical temperature T_m^{cr} of the F-F FGM beams with the power law index n, for some specified values of T_r and L. Some critical temperatures are also listed in Tables 3 and 4 simultaneously. As shown in these figures and tables, critical temperatures decrease with the increase of n. It means that the abilities of FGM beams to withstand critical temperature decreases as n increases. This is due to the fact that the component of Ti-6Al-4V increase with the increase of n, which leads to decreases of Young's modulus, tangent modulus and thermal expansion coefficient of FGM beams. In addition, it shows that the critical buckling temperatures drop significantly as the slenderness ratio L increases. This is because the bending stiffness of FGM beams decrease as the radio L increases.

Fig. 8(a, b) demonstrate influences of the gradient properties of materials on critical temperatures for the F-P FGM beams. Some critical temperatures are also listed in Table 5. It shows that the critical buckling temperatures decrease with the increase of n. And the critical buckling temperatures decrease with the increase of slenderness ratio L, as expected. Comparing with Fig. 7(a–c), the critical buckling temperatures for the F-F boundary conditions are higher than the F-P beams, when the same parameters n and L are given. As temperature ratio $T_r = T_m/T_c$ increases, the critical bucking temperatures obviously drop.

6. Conclusion

The elastoplastic thermal buckling of metal-ceramic FGM beams is studied by symplectic method in Hamiltonian system. In which the effective elastoplastic material properties of FGM are calculated according to TTO model. The buckling mode equations and bifurcation conditions are established and solved by analytical methods in the Hamiltonian system. The buckling thermal loads and buckling modes are obtained accordingly. The critical buckling temperatures can be obtained via yield condition and inverse solutions of buckling thermal axial forces. The following conclusions are obtained:

(1) The elastic thermal buckling usually occurs for FGM beams with large slenderness ratio. However, the elastoplastic thermal buckling occurs for FGM beams with small slenderness ratio. At the same time, the critical temperatures decrease as slenderness ratio increases.
(2) For the FGM beams with smaller slenderness ratio, elastoplastic buckling occurs when power law index is greater than some certain values; otherwise there are only failures of strength. The elastoplastic critical thermal axial forces decrease with the power law index increases, because the increment of metal constituent lead to drop in bending stiffness.
(3) Along the thickness of FGM beams, the effect of plastic flow is more dominating in the metal-rich side. The area of plastic flow zone

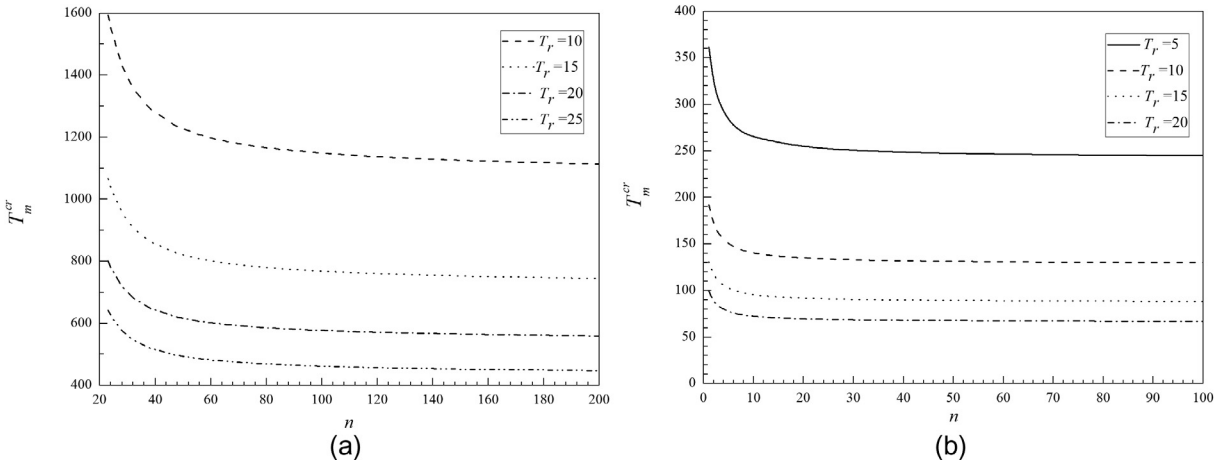

Fig. 8. The elastoplastic critical temperature T_m^{cr} of the F-P FGM beams versus power law index n. (a) $L = 5$, (b) $L = 10$.

Table 5
N_{cr}^{T} and T_{m}^{cr} of the F-P FGM beam with $L = 10$.

n		2	8	20	35	50	60	80	100
$N_{cr}^{T}(\times 10^{6}\mathrm{N})$		102.56	85.55	81.09	79.54	78.90	78.64	78.33	78.13
T_{m}^{cr} (K)	$T_r = 5$	533.53	443.50	421.90	411.88	407.57	405.83	403.79	402.26
	$T_r = 10$	281.79	233.41	222.11	216.94	214.73	213.84	212.78	212.02
	$T_r = 15$	191.45	158.39	150.73	147.25	145.76	145.17	144.45	143.94
	$T_r = 20$	144.98	119.86	114.08	111.45	110.33	109.88	109.34	108.96

significantly affected by slenderness ratio, power law index and elastoplastic material properties when the elastoplastic thermal buckling of FGM beams occurs, and it can be enlarged by decreasing the slenderness ratio or increasing the power law index.

Acknowledgments

This work was supported by the National Natural Science Foundation of China (grant numbers 11662008, 11862012) and the abroad exchange funding for young backbone teachers of Lanzhou University of Technology.

References

[1] Van PP, Thai CH, Xuan HN, Wahab MA. Porosity-dependent nonlinear transient responses of functionally graded nanoplates using isogeometric analysis. Compos Part B-Eng 2019;164:215–25.
[2] Thai CH, Ferreira AJM, Van PP. Size dependent free vibration analysis of multilayer functionally graded GPLRC microplates based on modified strain gradient theory. Compos Part B-Eng 2019. https://doi.org/10.1016/j.compositesb.2019.02.048.
[3] Sun Y, Li SR, Batra RC. Thermal buckling and post-buckling of FGM Timoshenko beams on nonlinear elastic foundation. J Therm Stresses 2016;39(1):11–26.
[4] Li SR, Zhang JH, Zhao YG. Thermal post-buckling of functionally graded material Timoshenko beams. Appl Math Mech 2006;27(6):803–10.
[5] Li SR, Zhang JH, Zhao YG. Nonlinear thermomechanical post-buckling of circular FGM plate with geometric imperfection. Thin Wall Struct 2007;45(5):528–36.
[6] Tran LV, Van PP, Lee J, Wahab MA, Xuan HN. Isogeometric analysis for nonlinear thermomechanical stability of functionally graded plates. Compos Struct 2016;140:665–7.
[7] Feldman E, Aboudi J. Buckling analysis of functionally graded plates subjected to uniaxial loading. Compos Struct 1997;38(1–4):29–36.
[8] Na KS, Kim JH. Three-dimensional thermomechanical buckling analysis for functionally graded composite plates. Compos Struct 2006;73(4):413–22.
[9] Liew KM, Yang J, Kitipornchia S. Postbucking of piezoelectric FGM plates subject to thermo-electro-mechanical loading. Int J Solids Struct 2003;40(15):3869–92.
[10] Ma LS, Wang TJ. Relationships between axisymmetric bending and buckling solutions of FGM circular plates based on third-order plate theory and classical plate theory. Int J Solids Struct 2004;41(1):85–101.
[11] Najafizadeh MM, Eslami MR. First order theory based thermoelastic stability of functionally graded material circular plates. AIAA J 2012;40(7):1444–50.
[12] Sun J, Xu X, Lim CW. Accurate symplectic space solutions for thermal buckling of functionally graded cylindrical shells. Compos Part B-Eng 2013;55(9):208–14.
[13] Sun J, Xu X, Lim CW. Buckling of functionally graded cylindrical shells under combined thermal and compressive loads. J Therm Stresses 2014;37(3):340–62.
[14] Ng TY, Lam KY, Liew KM, Reddy JN. Dynamic stability analysis of functionally graded cylindrical shells under periodic axial loading. Int J Solids Struct 2001;38(8):1295–309.
[15] Sofiyev AH. The stability of functionally graded truncated conical shells subjected to aperiodic impulsive loading. Int J Solids Struct 2004;41(13):3411–24.
[16] Sofiyev AH. The buckling of functionally graded truncated conical shells under dynamic axial loading. J Sound Vib 2007;305(4):808–26.
[17] Sofiyev AH, Deniz A, Akçay IH, Yusufoğlu E. The vibration and stability of a three-layered conical shell containing an FGM layer subjected to axial compressive load. Acta Mech 2006;183(3–4):129–44.
[18] Sohn KJ, Kim JH. Structural stability of functionally graded panels subjected to aero-thermal loads. Compos Struct 2008;82(3):317–25.
[19] Prakash T, Sundararajan N, Ganapathi M. On the nonlinear axisymmetric dynamic buckling behavior of clamped functionally graded spherical caps. J Sound Vib 2007;299(1):36–43.
[20] Ganapathi M. Dynamic stability characteristics of functionally graded materials shallow pherical shells. Compos Struct 2007;79(3):338–43.
[21] Shariyat M. Dynamic thermal buckling of suddenly heated temperature-dependent FGM cylindrical shells, under combined axial compression and external pressure. Int J Solids Struct 2008;45(9):2598–612.
[22] Shariyat M. Vibration and dynamic buckling control of imperfect hybrid FGM plates with temperature- dependent material properties subjected to thermo-electro-mechanical loading conditions. Compos Struct 2009;88(2):240–52.
[23] Ke LL, Wang YS. Size effect on dynamic stability of functionally graded microbeams based on a modified couple stress theory. Compos Struct 2011;93(2):342–50.
[24] Huang H, Han Q. Nonlinear dynamic buckling of functionally graded cylindrical shells subjected to time-dependent axial load. Compos Struct 2010;92(2):593–8.
[25] Zhang JH, Li SR. Dynamic buckling of FGM truncated conical shells subjected to non-uniform normal impact load. Compos Struct 2010;92(12):2979–83.
[26] Ghiasian SE, Kiani Y, Eslami MR. Dynamic buckling of suddenly heated or compressed FGM beams resting on nonlinear elastic foundation. Compos Struct 2013;106(12):225–34.
[27] Huang H, Han Q. Elastoplastic buckling of axially loaded functionally graded material cylindrical shells. Compos Struct 2014;117:135–42.
[28] Zhang Y, Huang H, Han Q. Buckling of elastoplastic functionally graded cylindrical shells under combined compression and pressure. Compos Part B-Eng 2015;69(69):120–6.
[29] Huang HW, Chen B, Han Q. Investigation on buckling behaviors of elastoplastic functionally graded cylindrical shells subjected to torsional loads. Compos Struct 2014;118(1):234–40.
[30] Xu G, Huang H, Han Q. Study on postbuckling of axial compressed elastoplastic functionally graded cylindrical shells. Mech Adv Mater Struct 2018;25(10):820–8.
[31] Sharma K, Kumar D. Elastoplastic analysis of FGM plate with a central cutout of various shapes under thermomechanical loading. J Therm Stresses 2017;40(11):1417–41.
[32] Sharma K, Kumar D. Elastoplastic stability and failure analysis of FGM plate with temperature dependent material properties under thermomechanical loading. Lat Am J Solids Struct 2017;14(7):1–26.
[33] Trinh TH, Nguyen DK, Gan BS, Alexandow S. Post-buckling responses of elasto-plastic FGM beams on nonlinear elastic foundation. Struct Eng Mech 2016;58(3):515–32.
[34] Van PP, Ferreira AJM, Xuan HN, Wahab MA. An isogeometric approach for size-dependent geometrically nonlinear transient analysis of functionally graded nanoplates. Compos Part B-Eng 2017;118:125–34.
[35] Zhang JH, Li GZ, Li SR, Ma YB. DQM-based thermal stresses analysis of functionally graded cylindrical shell under thermal shock. J Therm Stresses 2015;38(9):959–82.
[36] Zhang JH, Pan SC, Chen LK. Dynamic thermal buckling and postbuckling of clamped–clamped imperfect functionally graded annular plates. Nonlinear Dyn 2019;95:565–77.
[37] Huang H, Han Q. Stability of pressure-loaded functionally graded cylindrical shells with inelastic material properties. Thin Wall Struct 2015;92:21–8.
[38] Chu HJ, Xu XS, Lim CW, Jiang N, Ma JQ. Non-linear thermal buckling of elastic beams and expanding method of symplectic eigensolutions. J Dalian Univ Technol 2011;51(1):1–6. (in Chinese).
[39] Kiani Y, Eslami MR. Thermal buckling analysis of functionally graded material beams. Int J Mech Mater Des 2010;6(3):229–38.
[40] Li SR, Zhou YH, Zheng XJ. Thermal post-buckling of a heated elastic rod with pinned-fixed ends. J Therm Stresses 2002;25(1):45–56.
[41] Huang H, Han Q. Nonlinear buckling and postbuckling of heated functionally graded cylindrical shells under combined axial compression and radial pressure.Int. J Nonlin Mech 2009;44(2):209–18.
[42] Nemat-Alla M, Ahmed KIE, Hassab-Allah I. Elastic–plastic analysis of two-dimensional functionally graded materials under thermal loading. Int J Solids Struct 2009;46(14):2774–86.